Secondary Structure of a KCNE Cytoplasmic Domain

Jessica M. Rocheleau, Steven D. Gage, and William R. Kobertz

Department of Biochemistry and Molecular Pharmacology, University of Massachusetts Medical School, Worcester, MA 01605

Type I transmembrane KCNE peptides contain a conserved C-terminal cytoplasmic domain that abuts the transmembrane segment. In KCNE1, this region is required for modulation of KCNQ1 K^+ channels to afford the slowly activating cardiac I_{Ks} current. We utilized alanine/leucine scanning to determine whether this region possesses any secondary structure and to identify the KCNE1 residues that face the KCNQ1 channel complex. Helical periodicity analysis of the mutation-induced perturbations in voltage activation and deactivation kinetics of KCNQ1-KCNE1 complexes defined that the KCNE1 C terminus is α-helical when split in half at a conserved proline residue. This helical rendering assigns all known long QT mutations in the KCNE1 C-terminal domain as protein facing. The identification of a secondary structure within the KCNE1 C-terminal domain provides a structural scaffold to map protein–protein interactions with the pore-forming KCNQ1 subunit as well as the cytoplasmic regulatory proteins anchored to KCNQ1–KCNE complexes.

The Journal of General Physiology

INTRODUCTION

KCNE type I transmembrane peptides are a class of membrane-embedded β subunits that assemble with and modulate the function of voltage-gated K^+ channels (McCrossan and Abbott, 2004). The physiological importance of these small (~100–150 aa) β subunits on K^+ channel function is underscored by the genetic mutations in KCNE1 (E1) and KCNE2 (E2) that cause abnormalities in the cardiac rhythm (Splawski et al., 2000). Outside of the heart, mutations in E1 also cause endolymphatic collapse in the developing ear, and a C-terminal mutation in KCNE3 (E3) has been implicated in periodic paralysis since it alters Kv3.4 channel function (Letts et al., 2000; Abbott et al., 2001). All five KCNE peptides have been shown to assemble with and differentially modulate KCNQ1 (Q1) K^+ channels (McCrossan and Abbott, 2004). Q1–E1 complexes produce the slowly activating and deactivating cardiac I_{Ks} current, whereas Q1 assembly with either E2 or E3 gives rise to constitutively conducting complexes that rapidly activate and deactivate. Complexes with E4 and E5 slow the activation kinetics of Q1 channels similarly to E1; however, coassembly with these recently discovered KCNEs results in K^+ channel complexes that conduct only at extremely depolarizing potentials. Q1–KCNE complex gating is also modulated by several intracellular proteins. Calmodulin, PKA, protein phosphatase I, and A-kinase anchoring proteins are all cytoplasmic proteins that interact with membrane-embedded Q1–KCNE complexes (Marx et al., 2002; Kurokawa et al., 2003; Shamgar et al., 2006).

Although KCNE peptides modulate Q1 function differently, four KCNE peptides share a conserved cytoplasmic sequence (~20 aa) that is adjacent to the transmembrane domain. Function–structure studies with E1 have shown that this domain is required for Q1 channel modulation (Takumi et al., 1991; Tapper and George, 2000). Moreover, one third of the known genetic missense point mutations in E1 that cause long QT syndrome reside in this cytoplasmic region (Splawski et al., 2000; Schulze-Bahr et al., 2001; Ma et al., 2003; Lai et al., 2005; Napolitano et al., 2005). Therefore, we used perturbation mutagenesis to determine whether this cytoplasmic domain possesses any secondary structure and to identify residues that face the Q1 channel complex. Alanine and tryptophan scanning have been previously used to examine the secondary structure and protein-facing residues of both water-exposed and membrane-embedded domains of voltage-gated K^+ channels (Monks et al., 1999; Hong and Miller, 2000; Li-Smerin et al., 2000a,b). Using alanine and leucine mutagenesis, we observed two distinct classes of E1 mutants: those that strongly shift the voltage dependence of activation favoring the closed state, and those that resemble the wild-type (WT) complex. Periodicity analysis of our results revealed that the cytoplasmic C-terminal domain of E1 is helical when broken into two segments separated by a proline residue. This suggests that either the E1 C terminus is a kinked α-helix or the helix experiences two different protein environments above and below this junction point. Moreover, this helical projection defines four out of four dysfunctional mutations that cause long QT syndrome as facing the Q1 channel

Correspondence to William R. Kobertz: william.kobertz@umassmed.edu

Abbreviations used in this paper: α-PI, α-periodicity index; E1–E5, KCNE1–KCNE5; HA, hemagglutinin A; Q1, KCNQ1; TEVC, two-electrode voltage clamp; WT, wild-type.

complex. Given that this C-terminal domain is conserved in all but one of the known KCNE peptides, our E1 results predict that E2, E3, and E5 will possess a domain with similar structure when associated with Q1 channel subunits. In total, these results provide a structural motif from which to interpret the link between Q1-KCNE gating and intracellular regulation.

MATERIALS AND METHODS

Mutagenesis and In Vitro Transcription

Human Q1 and E1 were subcloned into vectors containing the 5′ and 3′ UTRs from the *Xenopus* β-globin gene for optimal protein expression. Single point mutations were introduced into E1 using Quickchange site-directed mutagenesis (Stratagene) and confirmed by DNA sequencing of the entire gene. For all surface luminometry experiments, the hemagglutinin A (HA) tag, YPYDVPDYA, was incorporated into the N terminus of E1 between residues 22 and 23 (Wang and Goldstein, 1995). The cDNA plasmids were linearized by MluI digestion, and cRNA synthesized by run-off transcription using SP6 or T7 RNA polymerase (Promega).

Electrophysiology

Oocytes were surgically removed from *Xenopus laevis* and defolliculated using 2 mg/ml collagenase (Worthington Biochemical Corp.) in OR2 containing (in mM): 82.5 NaCl, 2.5 KCl, 1 $MgCl_2$, 5 HEPES, pH 7.4, for 75–90 min. Isolated oocytes were rinsed with and stored in ND96 bathing solution (ND96B) containing (in mM): 96 NaCl, 2 KCl, 1.8 $CaCl_2$, 1 $MgCl_2$, 5 HEPES, 50 μg/ml gentamicin (Sigma Aldrich), pH 7.4, at 18°C. Approximately 24 h after extraction, oocytes were microinjected with 27.6 nl total volume of cRNA containing Q1 (7.5 ng/oocyte) and E1 (3.75 ng/oocyte). After 3–6 d, currents were recorded using Warner Instrument (OC-725) two-electrode voltage clamp (TEVC) and the data were acquired with Digidata 1322A using pClamp 8 or 9 (Axon Instruments). Electrodes were filled with 3 M KCl, 5 mM EGTA, 10 mM HEPES, pH 7.6, and had resistance between 0.2 and 1.0 MΩ. For each experiment, oocytes were held at −80 mV in ND96 (in mM): 96 NaCl, 2 KCl, 0.3 $CaCl_2$, 1 $MgCl_2$, 5 HEPES, pH 7.4, and pulsed to a command potential of 40 mV. Oocytes injected with Q1 and WT or mutant E1 RNA were only recorded from if a 4-s pulse to 40 mV produced current >1 μA to ensure that currents were coming from exogenously injected channel complexes. Tail currents for activation curves were measured in KD98 (in mM): 98 KCl, 0.3 $CaCl_2$, 1 $MgCl_2$, 5 HEPES, pH 7.4. Oocytes were held at −80 mV, and the tail current protocol was a series of 4-s test pulses to potentials between −100 and + 60 mV in 10-mV increments. For severely right shifted mutants (F78A and Y81A), test pulses between −100 and + 80 mV were used.

Data Analysis

The amplitude of tail currents was measured 6 ms after repolarization to −80 mV and normalized such that the maximal current was equal to 1. Normalized tail currents were plotted versus the depolarized potential to produce activation curves for WT and mutant E1 channel complexes. Activation curves were fit to a Boltzmann function, $I/I_{max} = A2 + (A1 - A2) / (1 + e^{(V - V1/2)*(-zF/RT)})$, where I/I_{max} is the normalized tail current amplitude, $V_{1/2}$ is the midpoint of activation, z is the maximum slope, F is Faraday's constant, R is the gas constant, and T is temperature in Kelvin. The upper and lower asymptotes, A1 and A2, were left to vary, allowing data to be fit since Q1–E1 complexes did not fully activate in the voltage ranges that can be used with oocytes (Gage and Kobertz, 2004). The isochronal free energy of channel opening, $\Delta G_{iso,}$ was calculated for WT and each mutant Q1–E1 complex using the equation $\Delta G_{iso} = zFV_{1/2}$. For each mutant, $\Delta\Delta G_{iso}$ was calculated as $\Delta G_{iso}{}^{mutant} - \Delta G_{iso}{}^{WT}$. The deactivation time constant (τ_d) was measured by fitting the current at −80 mV after a 40-mV depolarization to a single exponential.

Periodicity Analysis

The periodicity of $\Delta\Delta G_{iso}$ was determined as previously reported by Swartz et al. using the following equation (Li-Smerin et al., 2000a):

$$P(\omega) = \sum_{j=1}^{n}[(V_j - \langle V\rangle)\sin(j\omega)] + \sum_{j=1}^{n}[(V_j - \langle V\rangle)\cos(j\omega)],$$

where P(ω) is the power spectrum as a function of angular frequency, ω, and was determined for E1 C-terminal segments of 7–10 residues where ‹V› is the average $|\Delta\Delta G_{iso}|$ for each segment, V_j is the $\Delta\Delta G_{iso}$ at position j, and n is the number of residues in a segment. Since α helices are defined as having 3.6 residues per turn, a peak angle at 100° indicates an ideal α-helix. Transmembrane helices have shown peak angles shifted to higher frequencies, and since this membrane-abutting C-terminal region is presumably an extension of the membrane-spanning helix, we centered our analysis at 105° (Rees et al., 1989; Li-Smerin et al., 2000a). The α-periodicity index (α-PI) is the average value of P(ω) in this helical range (90°–120°) relative to the average value of P(ω) over the entire power spectrum and is a quantitative assessment of helical character:

$$\alpha\text{-PI} = \left[1/30\int_{90°}^{120°} P(\omega)d\omega\right] / \left[1/180\int_{0°}^{180°} P(\omega)d\omega\right];$$

values for α-PI >2 are considered indicative of an α-helix. For mathematical analyses that necessitated the inclusion of the nonfunctional D76A mutant, a $\Delta\Delta G_{iso}$ value of 1 kcal/mol was used to maintain the α-PI and peak angle calculated for the K69–N75 segment.

Cell Surface Luminometry

The surface expression of HA-tagged E1 proteins was measured by luminometry (Zerangue et al., 1999). Oocytes were injected with 7.5 ng Q1 and 3.75 ng WT or mutant E1–HA. After 3–5 d, currents were recorded from a few oocytes expressing WT E1–HA complexes to ensure that functioning complexes were present at the cell surface. ND96 containing 1% BSA was used to block and wash oocytes, as well as dilute antibodies. Oocytes were cooled to 4°C, blocked for 30 min, and primary antibody (1 μg/ml rat monoclonal α-HA; Roche) was applied for 1 h at 4°C. Oocytes were washed (8 × 5 min), incubated for 40 min with secondary antibody (2 μg/ml α-rat $F(ab)_2$; Jackson ImmunoResearch Laboratories), and washed again (5 × 10 min). Oocytes were finally washed with ND96 containing no BSA for 1 h at 4°C, individually placed in wells with 50 μl of ND96 solution, and mixed with 50 μl of the SuperSignal ELISA Femto Maximum Sensitivity Substrate (Pierce Chemical Co.). The signal at 405 nm was integrated for 10 s after a 20-s delay using a Veritas Microplate luminometer (Turner Biosystems). Data is reported in relative light units (RLU).

RESULTS

The C-terminal sequence that abuts the predicted transmembrane domain of E1 has been shown to be vital for Q1 modulation (Tapper and George, 2000), which suggests that a protein–protein interaction exists between

Q1 and E1 in this region. To identify the C-terminal residues of KCNE peptides that face the Q1 channel complex and to determine whether this region possesses any secondary structure, we individually mutated each residue in E1 to alanine, expressed these mutants with Q1 channels in *Xenopus* oocytes, and measured the changes in Q1–E1 complex gating using TEVC. For native alanine residues, leucine was used to induce a perturbation; for native serine residues, both alanine and leucine mutants were examined.

Of the 19 E1 C-terminal residues examined, only one mutant, D76A, did not express current. This was expected given that the long QT mutation (D76N) and the equivalent mutation in rat affords a nonfunctional Q1 channel complex (Wang and Goldstein, 1995; Splawski et al., 1997; Bianchi et al., 1999). Currents elicited from voltage depolarizations of WT and representative mutant Q1–E1 complexes in high external K^+ are shown in Fig. 1 A. To compare the voltage gating of the WT and mutant Q1–E1 complexes, we generated activation curves by measuring the tail current after repolarization and plotted it versus the depolarization potential. Standard tail current analysis requires that the channel reaches equilibrium between the open and closed states before repolarization; however, Q1–E1 complexes do not reach equilibrium even after 90-s depolarizations (Takumi et al., 1988), which necessitated an isochronal (4 s) tail current measurement. Normalized tail currents were plotted against depolarization potentials and the resultant activation curves (Fig. 1 B) were fit to a Boltzmann equation. From the Boltzmann fit, the voltage of half maximal activation ($V_{1/2}$) and slope factor (z) were determined for WT and each mutant Q1–E1 complex (Table I). These parameters were used to calculate the isochronal free energy of Q1–E1 complex opening at zero voltage (ΔG_{iso}), and for each mutant, $\Delta\Delta G_{iso}$ was also determined ($\Delta G_{iso}{}^{mutant} - \Delta G_{iso}{}^{WT}$). As in previous perturbation studies (Monks et al., 1999; Hong and Miller, 2000; Li-Smerin et al., 2000a,b), we defined residues with a $|\Delta\Delta G_{iso}| > 1$ kcal/mol as high impact. Using this arbitrarily defined cutoff, nine mutants scored as high impact, all of which resulted in stabilization of the closed state and acceleration of the deactivation kinetics when compared with WT. For the native serine residues, where alanine and leucine substitutions were individually examined, both S68A and S68L were defined as high impact, only S74L scored as high impact, and both S84 mutants were low impact.

To determine whether there was a periodicity of high and low impact mutants, the C-terminal residues were plotted on a helical wheel (Fig. 2, center). An α-helical pattern was not immediately apparent by simple visual inspection, nor by Fourier periodicity analysis (vide infra). While plotting our data on a helical wheel diagram, we initially observed a helical pattern for the bottom half of the region that abruptly disappeared conspicuously after a proline residue. Proline disruption of helical segments has been previously detected in transmembrane segments of two voltage-gated K^+ channels by perturbation mutagenesis (Hong and Miller, 2000; Li-Smerin et al., 2000a). Therefore, we plotted amino acids above and below the proline on two separate helical diagrams. The residues on the bottom helical wheel (Fig. 2, right) segregated into two distinct faces. Clustering of the high and low impact residues was also observed for the top helical diagram (Fig. 2, left); however, there were two high impact serines (S68 and S74) and the nonfunctional mutant (D76A) that warranted further experimental investigation.

S68A is a noticeable outlier in the top helical wheel landing in the low impact face. Sequence analysis indicates that S68 is within a putative PKC consensus sequence, suggesting that this serine may be phosphorylated. Since the premise of perturbation mutagenesis is that alterations in side chain volume lead to disruption of protein–protein interactions and thus channel function, we wondered whether S68A scored as high impact due to the inability to posttranslationally place a negative charge at this position, and not due to a change in side chain volume. To test this hypothesis, we mutated S68 to aspartic and glutamic acid, two commonly used imperfect isosteres of phoshorylated serine.

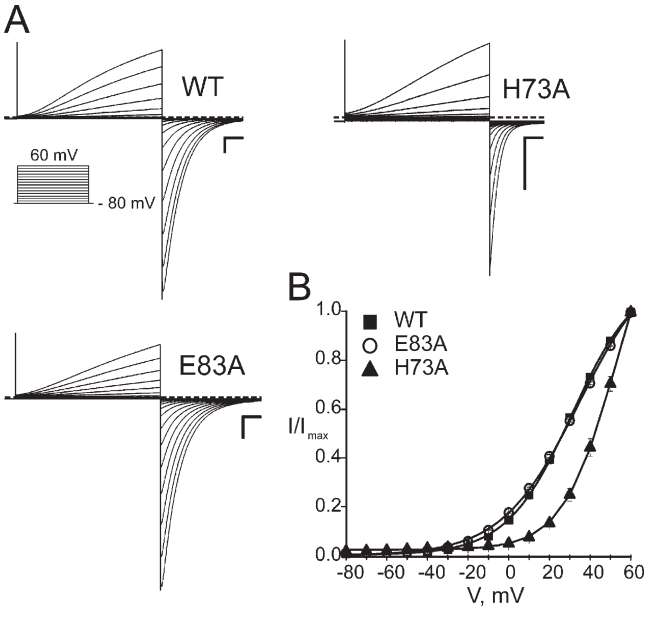

Figure 1. KCNE1 alanine mutants show diverse gating properties. (A) Two-electrode voltage clamp recordings of WT, H73A, and E83A mutant channels expressed in *Xenopus* oocytes. Currents were recorded in KD98 solution. Dashed line indicates zero current. Scale bars represent 1 μA and 0.5 s. Inset, protocol of 4-s depolarizations from −80 to 60 mV at 10-mV increments used to elicit currents shown. (B) Voltage activation curves for WT and representative mutant channel complexes calculated from tail current analysis. Solid curves represent Boltzmann fits to the data. Data was averaged from 5–10 oocytes each ± SEM.

TABLE I

Electrophysiological Properties of KCNE1 Mutants

Construct	$V_{1/2}$ (mV)	z	ΔG	ΔΔG	$\tau_{deactivation}$ (ms)
E1	31.3 ± 1.1	1.56 ± 0.03	1.02 ± 0.05	–	665 ± 80
S68A	60.0 ± 1.2	2.20 ± 0.06	3.04 ± 0.09	2.02 ± 0.10	131 ± 5
S68L	51.8 ± 1.6	1.90 ± 0.13	2.26 ± 0.15	1.24 ± 0.16	139 ± 7
S68D	43.6 ± 1.0	1.90 ± 0.07	1.91 ± 0.08	0.89 ± 0.09	156 ± 6
S68E	44.8 ± 1.0	2.05 ± 0.12	2.11 ± 0.09	1.09 ± 0.10	145 ±14
K69A	28.1 ± 1.6	1.84 ± 0.03	1.19 ± 0.06	0.17 ± 0.08	350 ± 28
K70A	56.1 ± 0.6	2.24 ± 0.06	2.90 ± 0.09	1.88 ± 0.10	105 ± 4
K70Q	54.5 ± 0.8	2.04 ± 0.08	2.27 ± 0.08	1.25 ± 0.09	132 ± 3
L71A	42.6 ± 2.6	2.04 ± 0.08	2.02 ± 0.18	1.00 ± 0.19	256 ± 16
E72A	43.0 ± 0.8	1.90 ± 0.02	1.88 ± 0.03	0.86 ± 0.06	362 ± 18
H73A	52.3 ± 3.2	2.03 ± 0.02	2.40 ± 0.10	1.38 ± 0.11	176 ± 3
S74A	34.1 ± 0.9	1.61 ± 0.03	1.27 ± 0.04	0.25 ± 0.06	496 ± 32
S74L	53.4 ± 1.5	1.94 ± 0.09	2.37 ± 0.09	1.35 ± 0.10	200 ± 12
S74I	44.4 ± 1.4	2.17 ± 0.03	2.22 ± 0.08	1.20 ± 0.09	189 ± 10
S74M	30.3 ± 2.1	1.90 ± 0.03	1.35 ± 0.11	0.33 ± 0.12	255 ± 22
N75A	27.9 ± 1.5	1.65 ± 0.02	1.06 ± 0.06	0.04 ± 0.08	644 ± 42
D76A	NF	NF	NF	NF	NF
P77G	ND	ND	ND	ND	ND
P77A	38.4 ± 2.7	1.65 ± 0.05	1.41 ± 0.08	0.39 ± 0.09	406 ± 9
P77L	39.5 ± 1.7	1.52 ± 0.08	1.38 ± 0.04	0.36 ± 0.06	381 ± 19
F78A	69.5 ± 6.4	1.50 ± 0.10	2.14 ± 0.12	1.12 ± 0.13	161 ± 14
N79A	45.6 ± 0.9	2.12 ± 0.04	1.98 ± 0.07	0.96 ± 0.09	179 ± 4
V80A	43.7 ± 1.3	1.55 ± 0.02	1.39 ± 0.04	0.37 ± 0.06	258 ± 13
Y81A	74.7 ± 1.0	1.85 ± 0.02	2.88 ± 0.15	1.86 ± 0.16	112 ± 3
I82A	59.4 ± 1.2	2.20 ± 0.03	2.67 ± 0.04	1.65 ± 0.06	145 ± 5
E83A	34.6 ± 0.8	1.34 ± 0.02	1.06 ± 0.02	0.04 ± 0.05	630 ± 50
S84A	44.6 ± 1.2	1.90 ± 0.06	1.95 ± 0.05	0.93 ± 0.05	317 ± 16
S84L	37.5 ± 4.2	1.13 ± 0.03	0.97 ± 0.09	−0.05 ± 0.10	449 ± 52
D85A	48.0 ± 2.5	1.98 ± 0.04	2.18 ± 0.13	1.16 ± 0.14	297 ± 20
A86L	24.8 ± 0.8	1.61 ± 0.03	0.92 ± 0.03	−0.10 ± 0.06	874 ± 57

Data from individual activation curves and deactivation time constants in KD98, obtained from 4–12 oocytes. Activation curves were fit to a Boltzmann function as described in Materials and methods. $V_{1/2}$ is the voltage of half-maximal activation and *z* is the slope factor. Time constants of deactivation were fit to a single exponential as described in Materials and methods. Values are mean ± SEM. NF, nonfunctional mutant; ND, no current detected.

Fig. 3 A shows the current–voltage relationships of the S68A, D, and E mutants. Activation curves (Fig. 3 B) show that substitution with either aspartic or glutamic acid had less of an effect ($\Delta\Delta G_{iso} \sim 1$ kcal/mol) than the alanine mutant ($\Delta\Delta G_{iso} \sim 2$ kcal/mol). If S68 is phosphorylated by PKC, mutation of the surrounding consensus sequence should also have a similar effect on Q1–E1 complex function. Substituting K70 with glutamine is predicted by oriented peptide libraries to disrupt the PKC consensus sequence (Nishikawa et al., 1997), yet this polar residue produces a nominal change in side chain volume. Like S68A, the K70Q mutant shifts the voltage dependence of activation of the Q1–E1 complex in favor of the closed state (Table I).

Of the native serines in the E1 C-terminal region, S74 was unique in that the alanine mutant was defined as low impact whereas the leucine mutant was high impact. Upon breaking the region in two halves, S74 was positioned at the high/low impact interface of the helical wheel (Fig. 2, left). We hypothesized that if S74 was at the water–protein interface, side chains with a higher degree of rotational freedom could use the adjacent aqueous environment to adopt a conformation that would maintain productive protein–protein interactions without steric clashes, whereas the more rigid, branched side chains could not. Conveniently, leucine, isoleucine, and methionine have approximately the same Van der Waals volume (Creighton, 1992), yet their flexibility and the three-dimensional space that they occupy is significantly different. Fig. 4 shows that mutating E1 S74 to the straight-chain methionine afforded a Q1 complex similar to WT, whereas mutation to the β-branched isoleucine resulted in a Q1–E1 complex similar to leucine, which was defined as high impact (Table I).

D76A was the only alanine mutation that did not express measurable current when coinjected with Q1 mRNA. There are two possibilities to explain the negligible

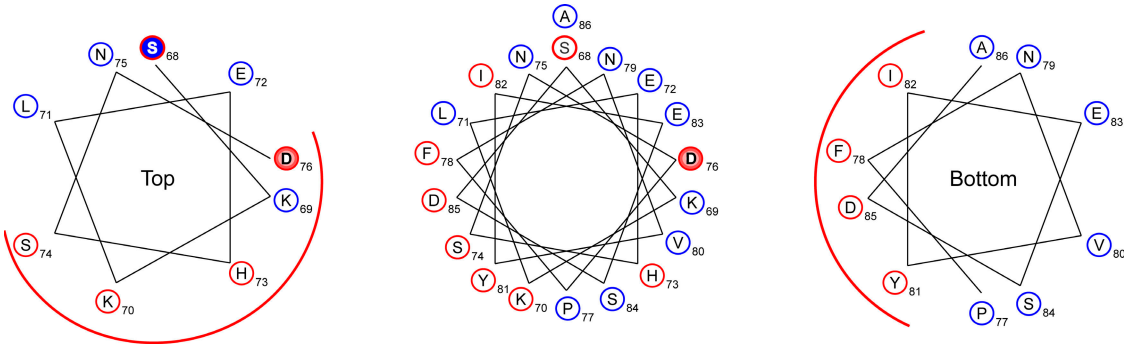

Figure 2. Periodicity of gating perturbations in the KCNE1 C-terminal domain. Center, helical wheel diagram of the 19 C-terminal E1 residues examined. Red circles indicate residues with $\Delta\Delta G_{iso} > 1$ kcal/mol, blue circles indicate $\Delta\Delta G_{iso} \leq 1$ kcal/mol. Power spectrum analysis indicates a peak angle of 125° and α-PI of 1.77 for the entire C-terminal segment. When residues above and below P77 are plotted on separate helical wheels (left and right), high impact residues (red) and low impact residues (blue) segregate to separate faces of each helical diagram. Each high impact face is denoted by a red line. S68A is a high impact residue on the low impact face (filled blue with red outline). D76A is a nonfunctional mutant at the plasma membrane, as determined by cell surface luminometry (red fill).

current observed with this mutation: (1) the Q1-D76A complex is nonfunctional; or (2) the Q1–D76A complex cannot reach the plasma membrane. To discern between these two, we used whole oocyte cell surface luminometry to determine whether an extracellularly HA-tagged version of D76A could reach the plasma membrane. Fig. 5 A shows that D76A protein is present at the plasma membrane similarly to WT and the long QT–causing mutant D76N, which has also been shown to be nonfunctional at the cell surface (Wang and Goldstein, 1995; Gage and Kobertz, 2004). Since the Q1–D76A complex is at the plasma membrane but not conducting, this mutant was scored as a high impact residue.

Splitting the E1 C-terminal region into two domains was based on our observation that the periodicity of high and low impact mutants shifted at P77, suggesting a kink or turn at this position. To experimentally test whether the presence of a helix-breaking residue at this position was required for proper Q1–E1 complex function, we mutated this proline to amino acids that are known to either induce flexibility or maintain α-helicity. Both alanine and leucine are often found in helical regions and are considered helix inducing (Rohl et al., 1996). Substitution of either of these residues at position 77 produced Q1 complexes similar to WT (Table I). Exchanging the proline for the highly flexible glycine residue did not afford currents above uninjected controls.

The lack of an obvious trend with this mutagenic discourse prompted us to use Fourier transform periodicity analysis to determine the amount of helicity in each segment and the location of the helical phase change. This nonbiased analysis has been used to define the helical segments within an entire voltage-sensing domain of a mammalian K^+ channel (Li-Smerin et al., 2000a). Determining the periodicity of a region using a power spectrum requires a $\Delta\Delta G_{iso}$ value for every residue. To satisfy this requirement, we excluded D76A since it was nonfunctional and S68A given the uncertainty of the native state of this side chain in the functioning Q1–E1 complex. Fig. 5 B shows the power spectra for K69–N75 and P77–A86 when the E1 C-terminal region is broken into two halves at P77. Both spectra show a peak angle within the boundaries of helicity (90°–120°) and with α-periodicity index (α-PI) >2. These results are highly indicative of two helical domains (Fig. 5 C), as was observed using simple helical wheel models (Fig. 2). We then varied the position of the breakpoint to determine whether P77 was the ideal spot to divide the E1 C-terminal domain. Since we cannot assign a $\Delta\Delta G_{iso}$ value for D76A, we used a placeholder value for D76 to maintain the helical trajectory of the K69–N75 segment and asked whether this helical domain extended beyond this residue. Propagation of the domain to include P77 and F78 resulted in sharp drop in α-PI, indicating that residues past D76 should not be included in the top segment (Table II). For the bottom segment, the α-PI increased as the analysis was extended to include the proline while the peak angle remained consistent for a helix. However, inclusion of D76 using any high impact value >1 kcal/mol decreased the α-PI, indicating that this high impact residue was out of helical phase with the bottom segment. Taken together, dividing the entire E1 C-terminal domain at any position other than P77 resulted in less helical character for either the top or the bottom segments.

DISCUSSION

We have used perturbation mutagenesis and helicity analysis to identify secondary structural elements in the conserved cytoplasmic region of the E1 β-subunit. Previous perturbation studies have primarily relied on

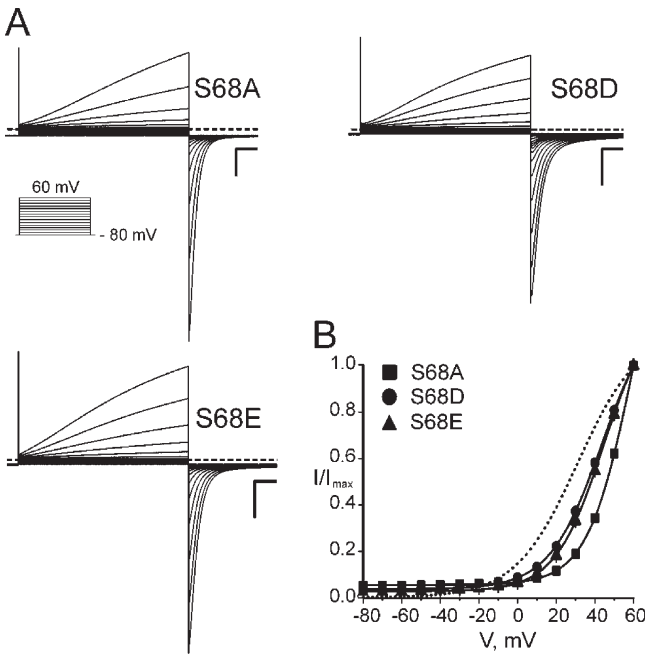

Figure 3. Negatively charged side chains produce smaller perturbations than alanine at position S68. (A) TEVC recordings of S68A and S68D channels expressed in *Xenopus* oocytes. Currents were recorded in KD98 solution. Dashed line indicates zero current. Scale bars represent 1 μA and 0.5 s. Inset, protocol of 4-s depolarizations from −80 to 60 mV at 10-mV increments used to elicit currents shown. (B) Voltage activation curves for S68A, S68D, and S68E mutant channels calculated from tail current analysis. Solid curves represent Boltzmann fits to the data. Dotted line indicates Boltzmann fit of WT activation curve. Data was averaged from 8–10 oocytes each ± SEM.

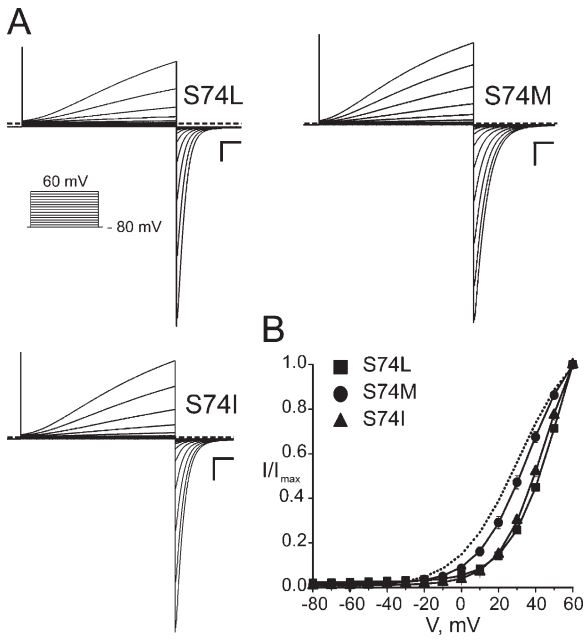

Figure 4. Branched amino acids cause larger perturbations at position S74. (A) TEVC recordings of S74L, S74M, and S74I channels expressed in *Xenopus* oocytes. Currents were recorded in KD98 solution. Dashed line indicates zero current. Scale bars represent 1 μA and 0.5 s. Inset, protocol of 4-s depolarizations from –80 to 60 mV at 10-mV increments used to elicit currents shown. (B) Voltage activation curves for S74 mutant channels calculated from tail current analysis. Solid curves represent Boltzmann fits to the data. Dotted line indicates Boltzmann fit of WT activation curve. Data was averaged from 6–10 oocytes each ± SEM.

comparing the free energy of channel opening of mutant channels versus WT (Monks et al., 1999; Hong and Miller, 2000; Li-Smerin et al., 2000a,b). To use this parameter for Q1–E1 complexes, which do not reach equilibrium under standard-length test depolarizations, we measured isochronal ΔΔGs. Although these values are not free energies, they allowed for a comparative analysis of the effect of mutations in E1 on Q1 function. Half of the mutations studied in the E1 C terminus gave $|\Delta\Delta G_{iso}| > 1$ kcal/mol, an arbitrarily defined cutoff for a high impact residue, but an empirically supported definition (Monks et al., 1999; Hong and Miller, 2000; Li-Smerin et al., 2000a,b). Changes in deactivation kinetics have also been used to define high impact residues, though a specific cutoff value has not emerged from previous reports (Monks et al., 1999; Hong and Miller, 2000). Graphing the deactivation kinetics of the E1 mutants reveals that a threefold acceleration of channel closing rate mirrors the trend observed with isochronally measured $\Delta\Delta G_{iso}$ (Fig. 5 D). Only one mutant, D76A, was refractory from this straightforward functional analysis since it did not generate measurable currents. However, cell surface labeling experiments show that this mutant is at the plasma membrane and is nonfunctional, and thus we can define it as high impact. Although only two mutations (D76A and the long QT causing D76N) have been examined at this position, it is interesting that both substitutions render the Q1–E1 complex nonfunctional, yet the complex traffics to the plasma membrane efficiently.

Plotting the residues on helical wheel resulted in no obvious clustering of high impact residues (Fig. 2, center). Periodicity analysis using a power spectrum confirmed that no helical pattern was present; both the peak angle (125°) and α-PI (1.77) were inconsistent with the region being a continuous helix. However, breaking the cytoplasmic region into two domains at a conserved proline (P77) segregated the high and low impact residues to distinct faces on helical wheels. In addition, Fourier periodicity analysis indicates that both domains have significant helical character (Table II), which supports the arbitrarily defined 1 kcal/mol cutoff value used for the helical wheel diagrams (Fig. 2). Moreover, this depiction places all known long QT mutants in this region on the high impact face. Given that the mutants in the high impact face markedly shift the gating of Q1–E1 complexes, we predict that these residues directly interact with the channel complex. This prediction is supported in high resolution detail with the crystal

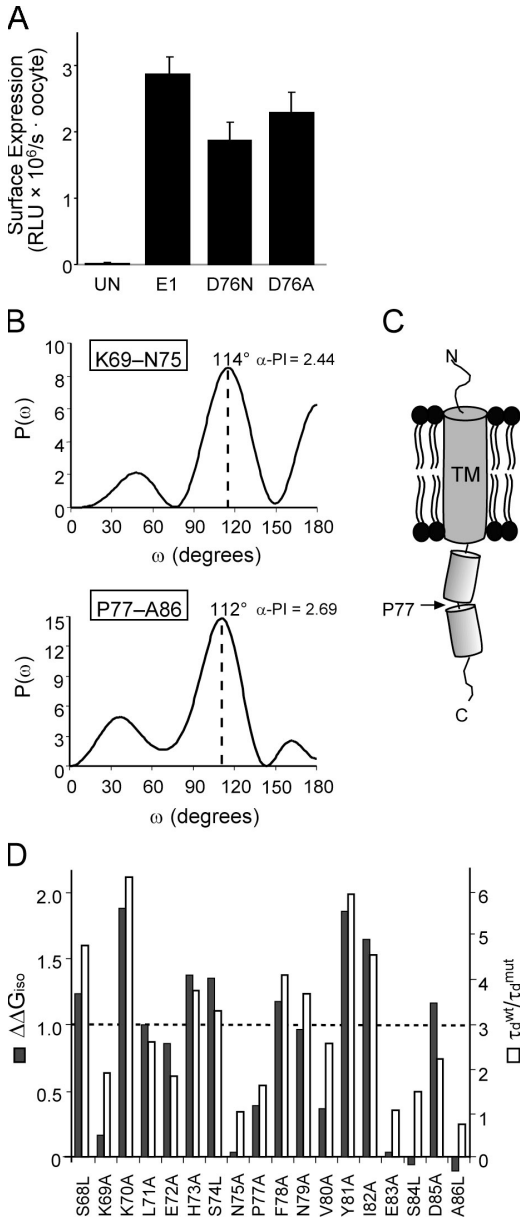

Figure 5. The transmembrane-abutting C-terminal domain is comprised of two helical regions. (A) Whole oocyte luminometry was used to quantify the surface expression of HA-tagged E1 peptides (E1, D76N, D76A) and uninjected controls (UN). Luminescence is reported in relative light units (RLU). Error bars represent SEM from 10–20 oocytes. (B) Periodicity analysis of the top (K69–D76) and bottom (P77–A86) segments of the E1 C-terminal domain. P(ω) is plotted as a function of angular frequency (ω) to generate a power spectrum of the $\Delta\Delta G_{iso}$ values for each segment. A value of 1 kcal/mol was assigned for the nonfunctional D76A mutant. The primary peak occurs at 114° for the top segment and 112° for the bottom. (C) A cartoon of the cytoplasmic E1 C-terminal domain split into two helical regions by a kink or turn. (D) Changes in deactivation rates mirror isochronal ΔΔG measurements for the E1 C-terminal domain mutants. Double bar graph comparing $\Delta\Delta G_{iso}$ and deactivation rates (τ_d) for the E1 C-terminal alanine and leucine mutants. Solid bars indicate $\Delta\Delta G_{iso}$, open bars $\tau_d^{WT}/\tau_d^{mutant}$. The dashed denotes the cutoff values for $\Delta\Delta G_{iso}$ and $\tau_d^{WT}/\tau_d^{mutant}$.

structures of voltage-gated K^+ channels (Jiang et al., 2003a,b; Long et al., 2005), which have verified that the high impact faces identified by previous perturbation studies are involved in protein–protein interactions within the voltage-sensing domain.

Although we observed a convincing pattern with helical wheel diagrams for the E1 C-terminal domain, S68A did not segregate to the high impact face, yet it had the highest $\Delta\Delta G_{iso}$ calculated. S68 is within a putative PKC consensus sequence. Disruption of the PKC site by mutation of the critical +2 basic residue (K70) to either glutamine or alanine resulted in Q1–E1 complexes with right-shifted activation curves similar to S68A, which cannot be phosphorylated. Although phosphorylation of E1 at this serine has not been observed experimentally, it has been detected in the homologous serine in E3 (Abbott et al., 2006). Substitution of S68 to either aspartic or glutamic acid, to mimic phosphoserine, showed that the more voluminous, but negatively charged side chains had less of an effect on Q1–E1 gating than the removal of hydroxyl group by alanine mutagenesis. These preliminary data suggest that E1 may be phosphorylated at S68, but requires further biochemical support and verification in native tissues.

Unlike S68 and S84, S74 was uniquely sensitive to changes in amino acid side chain volume in that only the bulkier S74L mutant scored as high impact. Helical analysis revealed that this residue was at the edge of the high impact face, which prompted us to experimentally examine whether this was the case. Isovoluminous substitution showed that branched amino acids (isoleucine, leucine) were less tolerated than the straight chain methionine side chain, which scored as a low impact residue using both criteria ($\Delta\Delta G_{iso}$ and τ_d). These results are consistent with the notion that S74 lies at the water–protein boundary since the flexible methionine side chain can adopt a productive protein–protein interaction between E1 and the Q1–channel complex while using the adjacent aqueous environment without energetic penalty.

Previous perturbation studies of voltage-gated K^+ channels had identified a proline residue in the S3 helix that disrupted the helical pattern of this transmembrane

TABLE II

α-Helical Characteristics of C-terminal E1 Segments

Segment	α-PI	Peak angle	Segment	α-PI	Peak angle
K69–N75	2.44	114°	P77 – A86	2.69	112°
K69–P77	1.61	123°	F78 – A86	2.53	109°
K69–F78	1.51	126°	N79 – A86	2.20	111°

Data from power spectrum periodicity analysis of $\Delta\Delta G_{iso}$ for residues in each segment. Power spectra, α-PI, and peak angle values were calculated as described in Materials and methods. For the top segments that contain D76, a placeholder value of 1 kcal/mol was used, which maintains the helical trajectory of the K69–N75 segment.

domain (Hong and Miller, 2000; Li-Smerin et al., 2000a). This functional analysis proposed that the S3 helix would be kinked at this proline residue, which was subsequently confirmed by three high resolution crystal structures of voltage-sensing domains (Jiang et al., 2003a,b; Long et al., 2005). Since our perturbation results afforded a strong helical pattern when the E1 C-terminal domain is divided in half at a proline residue, we hypothesized that P77 is inducing a kink or turn at this position. We attempted to mimic this kink by mutation to the helix breaking residue, glycine, but were unable to measure any currents above background when this mutant was expressed with Q1. To determine if the proline geometry was required for proper modulation of Q1 channels, we mutated P77 to alanine and leucine, two residues that have a high helix propensity (Rohl et al., 1996). When these mutants were expressed with Q1 subunits, K^+ currents and gating characteristics similar to WT Q1–E1 complexes were observed. Identical results (with alanine and tryptophan) were also obtained for the helix-kinking proline in the S3 segment of K^+ channel voltage sensors (Hong and Miller, 2000; Li-Smerin et al., 2000a), suggesting that detection of proline kinks using channel function and simple site-directed mutagenesis may not be possible. This conclusion is further supported by a systematic investigation of conserved proline residues in membrane proteins, which has shown that many protein–protein interfaces evolve ancillary interactions to stabilize kinked helices, thus obviating the need for proline residues to maintain the bent geometry (Yohannan et al., 2004).

Since mutagenesis could not elucidate whether a turn or kink was present at P77, we relied on power spectrum analysis to identify the location of the phase change in the E1 C-terminal domain. Using this mathematical approach, breaking the domain at P77 resulted in two segments with the greatest α-PI and peak angles most consistent with helices that are adjacent to transmembrane domains (Table II). This analysis indicates that the E1 C-terminal domain is helical with either a kink at P77 (Fig. 5 C) or the domain experiences a different protein environment above the proline residue, which may also be influenced by PKC phosphorylation. Sequence similarity of this membrane-abutting domain predicts that E2, E3 and E5 will possess a similar structural motif and protein environment when coassembled with Q1 subunits.

This conserved structural scaffold adds to the growing body of evidence that the E1 C-terminal domain is critical for Q1 channel modulation. Initial E1 deletion studies showed that removal of the membrane-abutting cytoplasmic domain eliminates the hallmark slow activation/deactivation kinetics of the Q1–E1 complex (Tapper and George, 2000). In addition, a recent E3 deletion study also concluded that the E1 C terminus was required for Q1 modulation, but not necessary for E3 modulation (Gage and Kobertz, 2004). Our alanine mutants also support this separation of KCNE modulation of Q1. Alanine mutants in E1 had significant effects on the voltage dependence and deactivation kinetics of Q1–E1 complexes, whereas the equivalent mutations in E3 had no measurable effect on the constitutively conducting Q1–E3 complex (unpublished data). Similarly, tryptophan mutants in the E1 transmembrane domain, though structurally informative, were consistently less perturbative on Q1–E1 complex function than C-terminal E1 alanine mutants (Goldstein, S.A.N., personal communication).

The cytoplasmic E1 C-terminal domain also provides a structural platform for potential interactions with tethered water soluble regulatory proteins. Calmodulin was recently shown to bind to the Q1 C terminus relatively close to the S6 transmembrane segment and facilitates channel assembly and calcium sensitivity (Shamgar et al., 2006). Adjacent to the Q1 calmodulin binding site is a leucine zipper sequence that is required for yotiao, an A-kinase anchoring protein, to bind (Marx et al., 2002). Anchoring of yotiao to the Q1 C terminus targets cAMP-dependent protein kinase (PKA) and protein phosphatase 1, which control the phosphorylation state of the Q1 N terminus. Moreover, this PKA-mediated modulation can be disrupted by genetic mutations within the E1 cytoplasmic domain (Kurokawa et al., 2003). Thus, the manifold nature of Q1–E1 complex regulation suggests that high impact regions identified in the C terminus of E1 may be revealing protein–protein interactions not only with Q1 α subunits, but also with tethered cytoplasmic regulatory proteins.

We thank Steve A.N. Goldstein for sharing his data with us prior to publication.

W.R. Kobertz thanks the Burroughs-Wellcome Foundation for a Career Award in the Biomedical Sciences that supported this work. This work was supported by National Institutes of Health GM0707650.

Angus C. Nairn served as editor.

Submitted: 29 August 2006
Accepted: 27 October 2006

REFERENCES

Abbott, G.W., M.H. Butler, S. Bendahhou, M.C. Dalakas, L.J. Ptacek, and S.A. Goldstein. 2001. MiRP2 forms potassium channels in skeletal muscle with Kv3.4 and is associated with periodic paralysis. *Cell.* 104:217–231.

Abbott, G.W., M.H. Butler, and S.A. Goldstein. 2006. Phosphorylation and protonation of neighboring MiRP2 sites: function and pathophysiology of MiRP2-Kv3.4 potassium channels in periodic paralysis. *FASEB J.* 20:293–301.

Bianchi, L., Z. Shen, A.T. Dennis, S.G. Priori, C. Napolitano, E. Ronchetti, R. Bryskin, P.J. Schwartz, and A.M. Brown. 1999. Cellular dysfunction of LQT5-minK mutants: abnormalities of IKs, IKr and trafficking in long QT syndrome. *Hum. Mol. Genet.* 8:1499–1507.

Creighton, T.E. 1992. Proteins: Structures and Molecular Properties. Second edition. W.H. Freeman and Company, New York. 512 pp.

Gage, S.D., and W.R. Kobertz. 2004. KCNE3 truncation mutants reveal a bipartite modulation of KCNQ1 K^+ channels. *J. Gen. Physiol.* 124:759–771.

Hong, K.H., and C. Miller. 2000. The lipid–protein interface of a Shaker K^+ channel. *J. Gen. Physiol.* 115:51–58.

Jiang, Y., A. Lee, J. Chen, V. Ruta, M. Cadene, B.T. Chait, and R. MacKinnon. 2003a. X-ray structure of a voltage-dependent K^+ channel. *Nature.* 423:33–41.

Jiang, Y., V. Ruta, J. Chen, A. Lee, and R. MacKinnon. 2003b. The principle of gating charge movement in a voltage-dependent K^+ channel. *Nature.* 423:42–48.

Kurokawa, J., L. Chen, and R.S. Kass. 2003. Requirement of subunit expression for cAMP-mediated regulation of a heart potassium channel. *Proc. Natl. Acad. Sci. USA.* 100:2122–2127.

Lai, L.P., Y.N. Su, F.J. Hsieh, F.T. Chiang, J.M. Juang, Y.B. Liu, Y.L. Ho, W.J. Chen, S.J. Yeh, C.C. Wang, et al. 2005. Denaturing high-performance liquid chromatography screening of the long QT syndrome-related cardiac sodium and potassium channel genes and identification of novel mutations and single nucleotide polymorphisms. *J. Hum. Genet.* 50:490–496.

Letts, V.A., A. Valenzuela, C. Dunbar, Q.Y. Zheng, K.R. Johnson, and W.N. Frankel. 2000. A new spontaneous mouse mutation in the Kcne1 gene. *Mamm. Genome.* 11:831–835.

Li-Smerin, Y., D.H. Hackos, and K.J. Swartz. 2000a. α-Helical structural elements within the voltage-sensing domains of a K^+ channel. *J. Gen. Physiol.* 115:33–50.

Li-Smerin, Y., D.H. Hackos, and K.J. Swartz. 2000b. A localized interaction surface for voltage-sensing domains on the pore domain of a K^+ channel. *Neuron.* 25:411–423.

Long, S.B., E.B. Campbell, and R. Mackinnon. 2005. Crystal structure of a mammalian voltage-dependent Shaker family K^+ channel. *Science.* 309:897–903.

Ma, L., C. Lin, S. Teng, Y. Chai, R. Bahring, V. Vardanyan, L. Li, O. Pongs, and R. Hui. 2003. Characterization of a novel Long QT syndrome mutation G52R-KCNE1 in a Chinese family. *Cardiovasc. Res.* 59:612–619.

Marx, S.O., J. Kurokawa, S. Reiken, H. Motoike, J. D'Armiento, A.R. Marks, and R.S. Kass. 2002. Requirement of a macromolecular signaling complex for β adrenergic receptor modulation of the KCNQ1-KCNE1 potassium channel. *Science.* 295:496–499.

McCrossan, Z.A., and G.W. Abbott. 2004. The MinK-related peptides. *Neuropharmacology.* 47:787–821.

Monks, S.A., D.J. Needleman, and C. Miller. 1999. Helical structure and packing orientation of the S2 segment in the Shaker K^+ channel. *J. Gen. Physiol.* 113:415–423.

Napolitano, C., S.G. Priori, P.J. Schwartz, R. Bloise, E. Ronchetti, J. Nastoli, G. Bottelli, M. Cerrone, and S. Leonardi. 2005. Genetic testing in the long QT syndrome: development and validation of an efficient approach to genotyping in clinical practice. *JAMA.* 294:2975–2980.

Nishikawa, K., A. Toker, F.J. Johannes, Z. Songyang, and L.C. Cantley. 1997. Determination of the specific substrate sequence motifs of protein kinase C isozymes. *J. Biol. Chem.* 272:952–960.

Rees, D.C., H. Komiya, T.O. Yeates, J.P. Allen, and G. Feher. 1989. The bacterial photosynthetic reaction center as a model for membrane proteins. *Annu. Rev. Biochem.* 58:607–633.

Rohl, C.A., A. Chakrabartty, and R.L. Baldwin. 1996. Helix propagation and N-cap propensities of the amino acids measured in alanine-based peptides in 40 volume percent trifluoroethanol. *Protein Sci.* 5:2623–2637.

Schulze-Bahr, E., M. Schwarz, S. Hauenschild, H. Wedekind, H. Funke, W. Haverkamp, G. Breithardt, O. Pongs, and D. Isbrandt. 2001. A novel long-QT 5 gene mutation in the C-terminus (V109I) is associated with a mild phenotype. *J. Mol. Med.* 79:504–509.

Shamgar, L., L. Ma, N. Schmitt, Y. Haitin, A. Peretz, R. Wiener, J. Hirsch, O. Pongs, and B. Attali. 2006. Calmodulin is essential for cardiac IKS channel gating and assembly: impaired function in long-QT mutations. *Circ. Res.* 98:1055–1063.

Splawski, I., M. Tristani-Firouzi, M.H. Lehmann, M.C. Sanguinetti, and M.T. Keating. 1997. Mutations in the hminK gene cause long QT syndrome and suppress IKs function. *Nat. Genet.* 17: 338–340.

Splawski, I., J. Shen, K.W. Timothy, M.H. Lehmann, S. Priori, J.L. Robinson, A.J. Moss, P.J. Schwartz, J.A. Towbin, G.M. Vincent, and M.T. Keating. 2000. Spectrum of mutations in long-QT syndrome genes. KVLQT1, HERG, SCN5A, KCNE1, and KCNE2. *Circulation.* 102:1178–1185.

Takumi, T., K. Moriyoshi, I. Aramori, T. Ishii, S. Oiki, Y. Okada, H. Ohkubo, and S. Nakanishi. 1991. Alteration of channel activities and gating by mutations of slow ISK potassium channel. *J. Biol. Chem.* 266:22192–22198.

Takumi, T., H. Ohkubo, and S. Nakanishi. 1988. Cloning of a membrane protein that induces a slow voltage-gated potassium current. *Science.* 242:1042–1045.

Tapper, A.R., and A.L. George Jr. 2000. MinK subdomains that mediate modulation of and association with KvLQT1. *J. Gen. Physiol.* 116:379–390.

Wang, K.W., and S.A. Goldstein. 1995. Subunit composition of minK potassium channels. *Neuron.* 14:1303–1309.

Yohannan, S., S. Faham, D. Yang, J.P. Whitelegge, and J.U. Bowie. 2004. The evolution of transmembrane helix kinks and the structural diversity of G protein-coupled receptors. *Proc. Natl. Acad. Sci. USA.* 101:959–963.

Zerangue, N., B. Schwappach, Y.N. Jan, and L.Y. Jan. 1999. A new ER trafficking signal regulates the subunit stoichiometry of plasma membrane K(ATP) channels. *Neuron.* 22:537–548.